

Partitioning and Interfacial Tracers for Differentiating NAPL Entrapment Configuration: Column-Scale Investigation

DONGPING DAI,
FRANK T. BARRANCO JR., AND
TISSA H. ILLANGASEKARE*

*Environmental Science and Engineering Division,
Colorado School of Mines, Golden, Colorado 80401*

Research on the use of partitioning and interfacial tracers has led to the development of techniques for estimating subsurface NAPL amount and NAPL–water interfacial area. Although these techniques have been utilized with some success at field sites, current application is limited largely to NAPL at residual saturation, such as for the case of post-remediation settings where mobile NAPL has been removed through product recovery. The goal of this study was to fundamentally evaluate partitioning and interfacial tracer behavior in controlled column-scale test cells for a range of entrapment configurations varying in NAPL saturation, with the results serving as a determinant of technique efficacy (and design protocol) for use with complexly distributed NAPLs, possibly at high saturation, in heterogeneous aquifers. Representative end members of the range of entrapment configurations observed under conditions of natural heterogeneity (an occurrence with residual NAPL saturation [discontinuous blobs] and an occurrence with high NAPL saturation [continuous free-phase LNAPL lens]) were evaluated. Study results indicated accurate prediction (using measured tracer retardation and equilibrium-based computational techniques) of NAPL amount and NAPL–water interfacial area for the case of residual NAPL saturation. For the high-saturation LNAPL lens, results indicated that NAPL–water interfacial area, but not NAPL amount (underpredicted by 35%), can be reasonably determined using conventional computation techniques. Underprediction of NAPL amount lead to an erroneous prediction of NAPL distribution, as indicated by the NAPL morphology index. In light of these results, careful consideration should be given to technique design and critical assumptions before applying equilibrium-based partitioning tracer methodology to settings where NAPLs are complexly entrapped, such as in naturally heterogeneous subsurface formations.

Introduction

The task of locating and characterizing nonaqueous-phase liquids (NAPLs) present in the subsurface at contaminated waste sites has presented significant challenges to scientists and engineers involved in site risk assessment and remediation. Traditional soil coring methods for NAPL assessments

(particularly denser than water NAPLs or DNAPLs) have proven to be ineffective as a result of NAPL remobilization during sampling (1) and the inability to deterministically resolve the spatial distribution of NAPL entrapment from localized, discrete samples. The difficult task of locating and characterizing subsurface occurrences of NAPL is compounded by the presence of aquifer heterogeneity, which will increase the complexity of NAPL movement and subsequent entrapment (2). The complex spatial distribution of NAPLs is controlled by unstable fingering (3), preferential channeling, and both micro- (pore) and macro-scale heterogeneity (layering and soil texture contrasts) of the subsurface formation (4–7). The final entrapment distribution in these complex geologic environments ranges from regions of low saturation (residual ganglia and blobs) to high saturation (free-phase pools and macro-scale entrapment zones resulting from capillary barriers).

Inherent difficulties with conventional NAPL characterization techniques have prompted the recent development of innovative, nondestructive techniques that utilize groundwater tracers for NAPL quantification and morphological evaluation (8–12). Scientific enthusiasm for, in particular, partitioning and interfacial tracers has led to the development of quantitative techniques for estimating NAPL amount (9, 13) and NAPL–water contact area (11, 14). Partitioning tracers, many of which are organic compounds themselves, reversibly partition (at equilibrium) to different degrees between NAPL and groundwater, resulting in the chromatographic separation of tracer signals observed at monitoring and/or extraction wells. Ideally, partitioning tracers behave conservatively during transport in the absence of NAPL, but their breakthrough would be retarded if NAPL were encountered. By measuring retardation of the partitioning tracers during displacement with a conservative tracer, the amount of NAPL within the tracer-swept region can be quantified (8, 12, 13, 15). Such compounds such as alcohols (6, 9, 12, 13, 16, 17), sulfur hexafluoride (18, 19), ^{222}Rn (20), and chlorofluorinated hydrocarbons (21–24) have been utilized as partitioning tracers for hydrocarbon detection and quantification.

Interfacial tracers are surface-active agents that adsorb and, therefore, accumulate at NAPL–water interfaces, leading to tracer retardation when compared with conservative tracers (11, 14, 25). By measuring retardation of the interfacial tracer relative to a conservative tracer, the NAPL–water interfacial area (a_{nw}) can be estimated if the adsorption isotherm for interfacial tracer accumulation is known. As demonstrated by Saripalli et al. (11) and Kim et al. (14), the Gibbs adsorption model can be employed to establish the nonlinear isotherm for monolayer interfacial adsorption given the data for the decrease in NAPL–water interfacial tension (γ_{nw}) with increasing concentration of interfacial tracer. Previous researchers have employed anionic surfactants, primarily sodium dodecyl benzene sulfonate (SDBS) and cetylpyridinium chloride (CPC), as interfacial tracers to characterize fluid–fluid interfacial areas in laboratory columns tracers (11, 14, 25) and field-scale applications (12).

The combined use of partitioning and interfacial tracers has been proposed as a robust technique for characterizing NAPL amount as well as entrapment distribution (11, 12). By determining NAPL saturation (S_n) with partitioning tracers and a_{nw} with interfacial tracers, a prediction of the spatial distribution and morphology of entrapped NAPL source regions can be made. Saripalli et al. (11) proposed that the ratio of interfacial area to volumetric NAPL content ($a_{\text{nw}}/\phi S_n$ where ϕ represents porosity), known as the NAPL morphology

* Corresponding author telephone: (303)384-2126; fax: (303)273-3311; e-mail: tillanga@mines.edu.

index (H_n), provides a measure of how NAPL is distributed within the porous medium.

Partitioning and interfacial tracer techniques were initially developed to assess the effectiveness of NAPL remediation technologies. In field investigations, such as partitioning interwell tracer tests (PITTs), tracers are deployed before and after cleanup implementation to assess remedial performance (13, 26–28). These techniques, as reported, have largely been tested and applied directly in the field where sufficient experimental control may not exist to gain a fundamental understanding of the processes and parameters that influence tracer behavior. Previous researchers have assumed that flowing groundwater containing the tracers effectively contacts all NAPL present in the soil and that instantaneous, equilibrium tracer partitioning and/or interfacial adsorption occurs. Controlled laboratory studies reported to date (9, 10, 11, 20, 25) have validated these theoretical assumptions as well as the resulting computational methods for use of partitioning and interfacial tracers in isotropic porous media at low NAPL saturation (up to approximately 0.2). Such experimental conditions are reflective of those expected for homogeneous aquifers following free NAPL removal but may have limited applicability to a variety of contaminated aquifer settings.

The primary goal of this laboratory study was to evaluate the behavioral diversity of partitioning, interfacial, and conservative tracers in water-saturated subsurface systems where NAPLs are entrapped under conditions of natural heterogeneity. To that end, representative end members of the range of entrapment configurations observed under natural soil heterogeneity (an occurrence with residual NAPL saturation [discontinuous blobs] and an occurrence with high NAPL saturation [continuous free-phase lens]) were simulated within controlled column-scale test cells. Subsequently, each occurrence type was subjected to partitioning and interfacial tracer tests to assess whether tracer evaluation could lead to accurate prediction of known NAPL quantity and distribution. Both entrapment types were prepared with the same volume of NAPL to evaluate the sole influence of NAPL distribution on tracer behavior. Existing theoretical assumptions and computational methods, which rely on instantaneous equilibrium partitioning, were employed to test their validity and relative error when applied to complex distributed NAPLs, such as the high-saturation NAPL lens.

Materials and Methods

Multiple tracer, laboratory, column-scale experiments (spatially 1-dimensional (1D) with respect to aqueous flow) were conducted with partitioning, interfacial, and nonreactive tracers to assess the objectives of this study. Multiple tracer experiments were preceded by measurement of batch NAPL–water partition coefficients and NAPL–water interfacial tension versus interfacial tracer concentration—important data for interpretation of measured tracer retardation. A description of experimental materials is followed by methodologies for batch partitioning and interfacial tension studies and multiple tracer column experiments.

Materials. Soltrol 220 (a nontoxic LNAPL mixture composed of C_{13} – C_{17} hydrocarbons; manufactured by Phillips 66 Company) was utilized as a representative NAPL within all experiments. Soltrol does not significantly partition into water or air; therefore, mass transfer of NAPL can be conveniently ignored during the experiments. The Soltrol was mixed with iodoheptane at a ratio of 9:1 (by volume), respectively, for the purpose of related research studies. Additionally, the NAPL was amended with a very low concentration of automate red dye for visual identification.

The alcohols, 1-hexanol, and 2,2-dimethyl-3-pentanol (DMP) (Sigma Chemical), were used as partitioning tracers throughout all experiments and were chosen to yield

breakthrough responses in a reasonably short time and yet ensure good separation of the partitioning and nonpartitioning tracers. Sodium dodecyl benzene sulfonate (SDBS) (Aldrich Chemical) was used as the interfacial tracer throughout experimentation. 2-Propanol and bromide (in the form of KBr) were utilized as nonreactive tracers.

Column experiments were performed with well-characterized, industrial-grade silica sand, ranging from fine to medium grain depending on the experiment. Two types of sorted sand (nos. 30 and 70) obtained from crushed sandstone (GRANUSIL silica sand by UNIMIN Corporation) were used to create the NAPL entrapment configurations studied. The saturated hydraulic conductivity of these sands, characterized in previous studies (29, 30), is 0.13 and 0.014 cm/s, respectively.

Batch-Partitioning Experiments. Batch-partitioning experiments were conducted to determine NAPL–water partition coefficients (K_{nw}) for the alcohols evaluated. Batch-partitioning tests, conducted in 16 mL, zero-headspace, septa-capped vials with equal volumes of NAPL and water, were conducted with 2-propanol, 1-hexanol, and DMP (initially added to the aqueous phase) ranging in concentration from 0 to 1000 mg/L. The vials were equilibrated by vigorous mixing on an orbital mixer for 24 h. This technique was similar to the “shake flask” method for determination of octanol–water partition coefficients; however samples of this study were mixed for a longer period of time. Following equilibration, a 2-mL aqueous sample was collected via syringe and placed into a 2-mL septa vial for alcohol analysis with a Hewlett-Packard (HP) 6890 gas chromatograph (GC). The GC was equipped with a 30.0 m long by 0.25 mm PAG capillary column (Supelco 2–4223) and a flame ionization detector (FID). The FID signal was acquired and integrated with a personal computer (PC) using HP Chemstation software.

The retardation factors of the partitioning and interfacial tracers and the measured NAPL–water partition coefficients were used to solve for the NAPL saturation at equilibrium conditions. Retardation factors were calculated from the zeroth and first temporal moment of the measured tracer breakthrough curves as described by Jin et al. (8):

$$R_{pt} = 1 + \frac{K_{nw}S_n}{(1 - S_n)} = \frac{t_p}{t_n} \quad (1)$$

where R_{pt} is the partitioning tracer retardation factor, K_{nw} is the linear partition coefficient (unitless), S_n is the residual NAPL saturation. The NAPL volume (V_n) was then calculated based on the S_n and the pore volume (V_e) as described by Jin et al. (8):

$$V_n = \frac{S_n V_e}{1 - S_n} \quad (2)$$

Tracer-estimated values of NAPL volume and NAPL–water interfacial area were used to compute the NAPL morphology index for these two occurrences (11) that defined the ratio of interfacial area to volumetric NAPL content. These estimates were compared with known values (based on test cell preparation procedures) to assess the ability of the tracers to accurately determine NAPL volume and distribution.

NAPL–Water Interfacial Tension (γ_{nw}) Measurements. NAPL–water interfacial tension (γ_{nw}) of Soltrol and aqueous solution containing SDBS was determined using the pendant drop method (31). NAPL drops were formed by suspending inverted droplets from a 2-mL micrometer syringe within a 30-mL deionized (DI) aqueous solution of set SDBS concentration (ranging from 0 to 270 mg/L). Each droplet was viewed through a contact angle goniometer (Rame-Hart, Inc.)

and photographed with an attached Polaroid camera. Droplet dimensions were measured from the photograph and used to calculate γ_{nw} . For each SDBS concentration evaluated, three duplicate pendants were measured. The calculated interfacial tensions were averaged to obtain a mean γ_{nw} as a function of SDBS concentration. General techniques specified by Saripalli et al. (11) were followed to determine NAPL–water interfacial tension (γ_{nw}) as a function of SDBS concentration. The local slope of this relationship ($\partial\gamma_{nw}/\partial C_{SDBS}$) at the initial SDBS concentration of injected tracer (i.e., 185 mg/L) within the test cells was used to determine the interfacial adsorption coefficient (K_i (cm)) as described by previous tracer studies in laboratory and field settings (11, 12, 14). Since K_i is dependent on the tracer concentration, this determination represents an approximation of the actual K_i value. K_i describes equilibrium SDBS adsorption at the NAPL–water interface. The approximate value of K_i was utilized, with tracer breakthrough data to compare the NAPL–water interfacial area (a_{nw}) between experiments using the following relationship (11):

$$R_{\text{fit}} = 1 + \frac{K_i a_{nw}}{\theta_w} \quad (3)$$

where R_{fit} is the interfacial tracer retardation factor (calculated from the zeroth and first temporal moment of the tracer breakthrough curve) and θ_w is the volumetric water content. The a_{nw} is the NAPL–water contact area per bulk volume (cm^2/cm^3). The approach used to estimate a_{nw} assumes that the NAPL–water interface is the only location for reversible SDBS adsorption and that this process is the sole contributor to the observed retardation. This assumption has been shown to be justified for SDBS use with clean sand media (11), as was the case for this study. Although it is recognized that the presence of nonequilibrium adsorption and/or partitioning between water and NAPL does not influence first moments (32) and, consequently, retardation, severe nonequilibrium could lead to underestimation of first moments because of difficulties in accurately characterizing extended tails of breakthrough curves. Because of nonequilibrium effects on the interfacial tracer, comparisons can only be drawn between experiments to determine relative changes in NAPL morphology.

Multiple Tracer Column-Scale Experiments. Experiments utilizing nonreactive (bromide and 2-propanol), partitioning (1-hexanol and DMP), and interfacial (SDBS) tracers were performed within rectangular 40 cm long by 5 cm high by 5 cm wide (internal dimensions) column-scale test cells composed of aluminum on all sides except for a 40 cm long by 5 cm high-gasketed Plexiglas visualization wall. Sidewalls were sealed with butyl rubber compressible gaskets and held together with counter-sunk allen screws. The influent and effluent ends of the test cell were fitted with 0.25 in. thick bronze frits for mixing solutes and creating constant boundary conditions. Procedures for column preparation, emplacement of NAPL, and tracer experimentation for the NAPL entrapment configurations assessed are discussed in chronological order of experimentation.

The test cell containing a high-saturation LNAPL lens was prepared by premixing a known volume of moist no. 30 sand with a known volume of NAPL to create an LNAPL saturation of 0.5. All metallic walls of the test cell were joined, leaving off only the Plexiglas wall for soil packing. On the inside of one of longitudinal walls, two 10 cm long by 5 cm wide by 1 cm high aluminum plates were sealed to the test cell to create a 20 cm long by 5 cm wide by 1 cm high channel (oriented parallel to the direction of aqueous flow) for NAPL emplacement. These plates served to prohibit lateral NAPL migration once cell construction was completed. The NAPL-containing sand was then spoon-filled transversely into the

20 cm long by 5 cm wide by 1 cm high channel, which was temporarily separated from the remainder of the test cell with a sheet metal barrier. The remainder of the test cell (on the opposing side of the sheet metal barrier) was wet packed with clean, water-saturated no. 70 sand. (Two sand types were used in this experiment to create a capillary barrier opposing NAPL migration from the high-saturation lens.) The sheet metal barrier was then gently removed, and the thin opening at the contact between NAPL- and water-containing sand was pressed shut by applying mild pressure to the sand surface. Subsequently, the Plexiglas wall was installed, and the test cell was placed horizontally (with the LNAPL accumulation vertically upward) within a flow apparatus. The flow apparatus was comprised of the test cell attached via stainless steel tubing to two, parallel-mounted, low-flow syringe pumps (Harvard Apparatus). Outflow from the test cell was directed via tubing to a sampling port open to the atmosphere.

To initiate testing, a multiple partitioning tracer test was performed to compare predicted with known NAPL volume. Flow of deionized water from one pump was established at an interstitial pore velocity of 18 cm/h in the test cell. Once steady-state conditions were achieved, flow was diverted without interruption to the other pump. At the same rate as initial flow, a finite pulse (1 PV) of an aqueous solution containing 200 mg/L bromide and 250 mg/L each of 2-propanol, 1-hexanol, and DMP was pumped through the cell. Following tracer injection, equal flow was routed back to DI water in the initial pump for the duration of the test (lasting 5 PV on average). Discrete 2-mL samples were collected intermittently (to reduce sample collection time and therefore minimize tracer volatilization) at 15-min intervals from the column effluent and analyzed for partitioning tracers with the previously described GC technique and analyzed for bromide by HPLC (Hewlett-Packard) equipped with an ion-exchange column.

Following the partitioning tracer test on this cell, an experiment was performed with the interfacial tracer, SDBS, and bromide to determine the NAPL–water contact area at the LNAPL lens surface. All experimental procedures and conditions for the interfacial tracer test were the same as for the partitioning tracer test, except that SDBS and bromide (at concentrations of 185 and 200 mg/L, respectively) were used rather than partitioning tracers. Both analytes were assessed by HPLC with an ion-exchange column as described previously (11, 12, 14).

After completing both partitioning and interfacial tracer tests on the high-saturation LNAPL lens, up to 10 pore vol of DI water was flushed through the test cell. Subsequently, the flow-through cell was prepared for tests on an occurrence with the same NAPL volume but now distributed in discontinuous blobs at residual saturation. The Plexiglas wall was removed from the cell. Without removing any media, the NAPL-containing sand from the lens was thoroughly mixed into adjacent clean sand, creating a homogeneous low NAPL saturation (0.10) within the mid-section of the cell (dimensions 20 cm long by 5 cm wide by 5 cm high). The Plexiglas wall was reinstalled, and tracer tests were initiated. Partitioning and interfacial tracer tests were then repeated on this NAPL entrapment configuration. All steps regarding methodology, procedures, and test conditions for partitioning and interfacial tracer tests were the same as for those of the high-saturation LNAPL lens.

Results and Discussion

Batch-Partitioning Experiments. The results of batch-partitioning experiments conducted to determine NAPL–water partition coefficients for the group of alcohols studied are shown in Figure 2. Results indicate that NAPL–water partitioning is linear with respect to alcohol concentrations

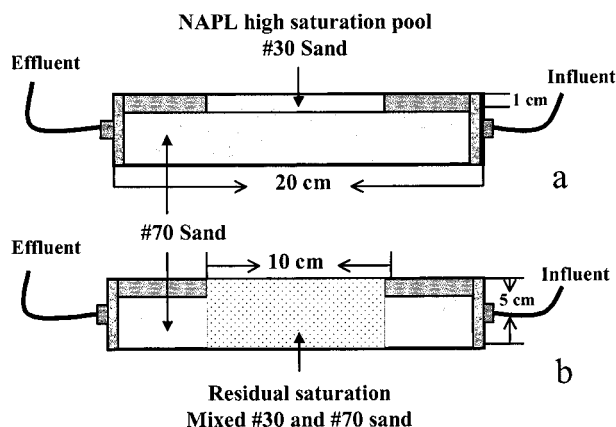


FIGURE 1. Schematic diagram of the column packing (a) high-saturation pool and (b) residual entrapment configurations.

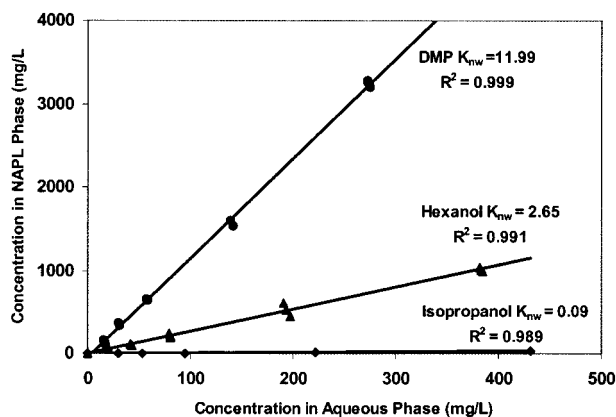


FIGURE 2. Linear partitioning of alcohol tracers between NAPL and water in the system studied. The partition coefficient reflected as the slope of the curve for 2-propanol, 1-hexanol, and DMP is 0.001, 3.0, and 12.0, respectively.

employed in this study. Measured partition coefficients, reflected as the slope of the linear trend, are constant with increasing aqueous tracer concentration. Based on these measurements, calculated NAPL–water partition coefficients for 2-propanol, 1-hexanol, and DMP were 0.01, 3.0, and 12.0, respectively. These data indicate an increasing Soltrol–water partition coefficient with increasing molecular weight of alcohol, with 2-propanol acting nearly conservative and DMP moderately partitioning. Measured partition coefficients were used in conjunction with measured partitioning tracer retardations to predict NAPL volume within the tracer-swept region.

NAPL–Water Interfacial Tension (γ_{nw}) Measurements.

The relationship between NAPL–water interfacial tension (γ_{nw}) and SDBS concentration is shown in Figure 3. The interfacial adsorption coefficient, calculated with knowledge of the local slope at the injected SDBS concentration (185 mg/L), was found to be 5.985×10^{-4} cm. This value was used later in conjunction with measured retardations from interfacial tracer tests to solve for a_{nw} of the NAPL occurrences that were studied.

Multiple Tracer Column Experiments. The results of partitioning and interfacial tracer tests for the NAPL entrapment configurations studied are shown in Figures 4 and 5 and summarized in Tables 1 and 2. The data in Figure 4 are also plotted in log scale and inserted in the figure for readers to better assess the tails of the BTCs. Hexanol breakthrough was retarded (1.2) but only slightly relative to bromide and 2-propanol. DMP retardation 1.87 was significant and, therefore, was used for subsequent predictions of NAPL mass/

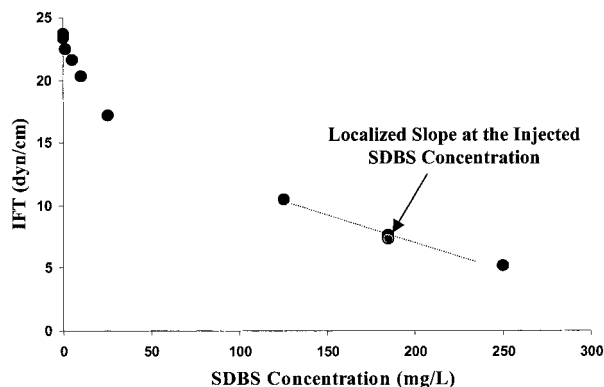


FIGURE 3. Measured relationship between NAPL–water interfacial tension and SDBS concentration. The local slope of this trend at the injected SDBS concentration (185 mg/L) was used to calculate the interfacial adsorption coefficient for determining NAPL–water interfacial area.

distribution and for comparisons of tracer data between NAPL entrapment configurations studied (Figures 4 and 5). In Figure 4, the data for DMP after 4 (for residual saturation) and 5 pore vol (for high-saturation entrapment) were extrapolated assuming a log-linear relationship. The DMP retardations for both cases were estimated based on the extrapolated breakthrough curves.

In Tables 1 and 2, measured versus predicted (based on known NAPL amount) partitioning tracer retardation is shown for the cases of homogeneously distributed residual NAPL saturation and the high-saturation LNAPL lens, respectively. Reasonable predictions of DMP retardation were made for the former case; the percent difference between measured and predicted values was only 1.1%, clearly indicating that equilibrium predictive assumptions are valid when NAPL is evenly distributed at low saturation. Inaccurate prediction resulted, however, for the case of the high-saturation LNAPL lens (Table 2). The percent difference between measured and predicted DMP retardation was approximately 35%. This significant difference is likely attributable to kinetic limitations to equilibrium partitioning behavior resulting from the lack of intimate contact between the aqueous flow field and the NAPL source zone. As a result of relative permeability reductions to water within the NAPL, aqueous flow largely bypassed this region, causing an earlier than expected partitioning tracer breakthrough (relative to equilibrium NAPL–water partitioning).

The influence of NAPL entrapment configuration on partitioning tracer behavior is clearly evident by the comparison of breakthrough curves for the case of homogeneously distributed residual NAPL saturation versus that of the high-saturation LNAPL lens (Figure 4). The retardation of DMP was 1.87 for the former case and only 1.52 for the latter. Yet, the same amount of NAPL was contained in both simulations. On the basis of measured retardation, 98% of NAPL mass was accounted for with the residual occurrence. Conversely, only 61% of the mass present in the LNAPL lens was estimated based on measured DMP retardation. This result clearly indicates that the retardation of tracers for the LNAPL lens is an underestimate, probably occurring in response to kinetic limitations to partitioning processes. Tracer partitioning for this occurrence was presumably controlled by rate-limited diffusion in to and out of the LNAPL lens. Certain aspects of the LNAPL lens breakthrough curve (Figure 4) support this presumption. For instance, the elongated DMP breakthrough tail indicates nonequilibrium partitioning of DMP from the LNAPL to the aqueous phase.

The influence of NAPL entrapment configuration on interfacial tracer behavior is also evident from a comparison of breakthrough curves for the case of homogeneously

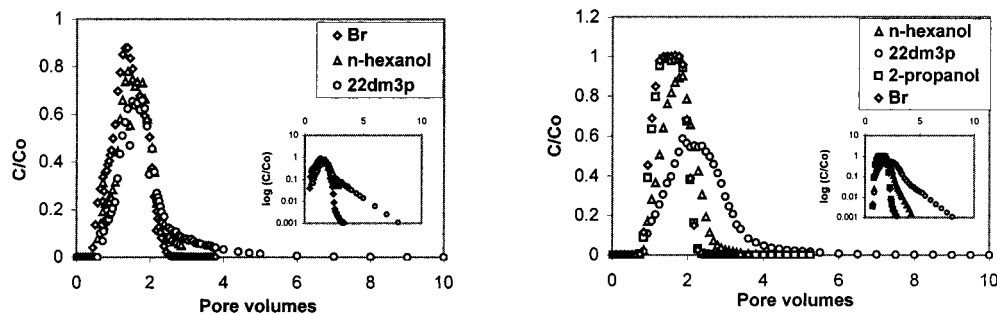


FIGURE 4. Influence of NAPL entrapment configuration on partitioning tracer breakthrough. The same mass of NAPL was used to create a homogeneously distributed residual NAPL saturation (on right) vs a high-saturation NAPL lens (on left). Note the significantly greater retardation for DMP on the former (1.86) (after 5 pore vol, the data were log-linear extrapolated) vs the latter (1.52) (after 4 pore vol, the data were log-linear extrapolated).

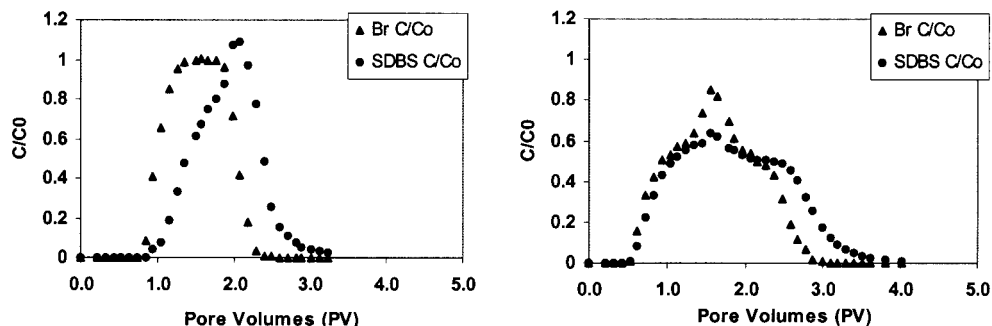


FIGURE 5. Influence of entrapment configuration on interfacial tracer breakthrough. The same mass of Soltrol was used to create a homogeneously distributed residual NAPL saturation (on left) vs a high-saturation NAPL lens (on right). Note the significantly greater retardation for SDBS on the former (1.38) vs the latter (1.23).

TABLE 1. Measured vs Predicted Partitioning Tracer Retardation for the Case of Homogeneously Distributed Residual NAPL Saturation^a

	measured retardation ^b	predicted retardation ^c	% difference ^d
2-propanol	1.03	1.00	2.9
<i>n</i> -hexanol	1.21	1.22	0.8
DMP	1.86	1.87	1.1

^a Residual NAPL saturation is 0.1. (Residual NAPL saturation for full column volume is 0.068.) ^b Measured in column-scale test cell at an interstitial velocity of 14.5 cm/h. ^c Predicted based on linear, reversible, equilibrium partitioning of tracers (see ref 8). ^d Percent difference between measured and predicted retardation.

TABLE 2. Measured vs Predicted Partitioning Tracer Retardation for the Case of a High-Saturation LNAPL Lens^a

	measured retardation ^b	predicted retardation ^c	% difference ^d	estd error for NAPL saturation (%)
2-propanol		1.00		
<i>n</i> -hexanol	1.16	1.22	5.1	23
DMP	1.52	1.87	35	35

^a LNAPL saturation in lens was 0.5. (Residual NAPL saturation for full-column volume is 0.068.) ^b Measured in column-scale test cell at an interstitial velocity of 14.5 cm/h. ^c Predicted based on linear, reversible, equilibrium partitioning of tracers (see ref 8). ^d Percent difference between measured and predicted retardation.

distributed residual NAPL saturation versus that of the high-saturation LNAPL lens (Figure 5). Both cases showed measurable retardation, which was used to calculate the NAPL-water interfacial area for each occurrence. Calculated interfacial areas were 281 (homogeneously distributed NAPL) and 168 cm²/cm³ (high-saturation LNAPL lens). These values are comparable with those in the literature from controlled

experiments (11, 14, 25). Considering that interfacial tracers only interact with the NAPL-water interface (and not diffuse through the bulk NAPL), this result is expected.

Calculated values of S_n and a_{nw} resulting from measured partitioning and interfacial tracer breakthrough curves were used to compute the NAPL morphology index (H_n) for the two NAPL occurrences assessed. H_n for the case of residual NAPL saturation was 10 500 cm²/cm³, whereas H_n for the case of a high-saturation LNAPL lens was 10 100 cm²/cm³. Saripalli et al. (11) and Annable et al. (12) have shown that high values of H_n indicate that NAPL may be spread out, perhaps as thin coatings on the solid matrix, thus providing large contact area between the NAPL and the aqueous phases, such as for the case of NAPL at residual saturation. In contrast, lower values of H_n may indicate that NAPL may be confined to isolated regions or patches of relatively high NAPL saturation, providing limited contact area, such as for the case of macro-entrapped NAPL ganglia (or pockets) and high-saturation NAPL pools or lenses. Results of this study do not verify the trend seen in these previous studies. No significant difference is observed between the residual and the high-saturation cases. This could be due to the underestimation of S_n (due to kinetically limited partitioning) for the high-saturated LNAPL lens resulting in an inaccurate value of H_n .

Implications of Findings

Results of this study indicate that the use of existing computational partitioning and interfacial tracer techniques, in particular, those relying on equilibrium assumptions, are not necessarily valid for determination of NAPL amount and distribution with complex NAPL entrapment configurations, such as macro-entrapped, high-saturation LNAPL lenses (and, presumably, DNAPL pools). Study results further indicate that if equilibrium assumptions are used for such mass transfer-limited systems, gross underestimation of NAPL amount and incorrect prediction of NAPL distribution will result. Kinetic limitations observed within laboratory,

column-scale test cells would be expected to play a more significant role in actual field situations where rate-limited tracer diffusion may be enhanced by natural subsurface heterogeneity. Rate limitations observed in the field, however, will be dependent on partitioning tracer diffusion coefficients as well as the thickness of NAPL zones through which partitioning tracers must diffuse. In light of the results of this study, careful consideration should be given to the design protocol, testing methodology, and computational assumptions used during field utilization of partitioning and interfacial tracer techniques. For instance, consideration should be given to tracer test optimization through spatially dependent injection, residence time control, and kinetic (as opposed to equilibrium) data assessment models.

Acknowledgments

Support for this research was provided by the U.S. Environmental Protection Agency through the Great Plains/Rocky Mountain Hazardous Substance Research Center at Kansas State University. Equipment support was through a National Science Foundation Major Research Instrumentation grant (9977708). We also gratefully acknowledge Dr. Todd Cort for editing this manuscript and Mr. Leslie Timian for assisting in the design and development of the laboratory testing equipment.

Literature Cited

- (1) Anderson, W. G. *J. Pet. Technol.* 1986, October, 1125.
- (2) Illangasekare, T. H.; Yates, D. N.; Armbruster, E. J. *J. Environ. Eng.* 1995, 121 (8), 571–579.
- (3) Held, R. J.; Illangasekare, T. H. *Water Resour. Res.* 1995, 31 (5), 1213–1222.
- (4) Schwille, F. *Dense Chlorinated Solvents in Porous and Fractured Media: Model Experiments*; Pankow, J. J., translator; Lewis Publishers: Boca Raton, FL, 1998; p 146.
- (5) Illangasekare, T. H.; Ramsey, J. L.; Jensen, K. H.; Butts, M. J. *Contam. Hydrol.* 1995, 20, 1–25.
- (6) Kueper, B. H.; Frind, E. O. *Water Resour. Res.* 1991, 27, 1049–1057.
- (7) Kueper, B. H.; Frind, E. O. *Water Resour. Res.* 1991, 27, 1059–1070.
- (8) Jin, M.; Delshad, M.; Dwarakanath, V.; McKinney, D. C.; Pope, G. A.; Sepehrnoori, K.; Tilburg, C. E. *Water Resour. Res.* 1995, 31 (5), 1201–1211.
- (9) Jin, M.; Butler, G.; Jackson, R. E.; Mariner, P. E.; Pickens, J. F.; Pope, G. A.; Brown, C. L.; McKinney, D. C. *Ground Water* 1997, 35 (6), 964–972.
- (10) Wilson, R. D.; Mackay, D. M. *Environ. Sci. Technol.* 1995, 29 (5), 1255–1258.

- (11) Saripalli, K. P.; Kim, H.; Rao, P. S. C.; Annable, M. D. *Environ. Sci. Technol.* 1997, 31 (3), 932–936.
- (12) Annable, M. D.; Jawitz, J. W.; Rao, P. S. C.; Dai, D. P.; Kim, H.; Wood, A. L. *Ground Water* 1998, 6 (3), 495–502.
- (13) Annable, M. D.; Rao, P. S. C.; Hatfield, W. D.; Graham, W. D.; Wood, A. L. *J. Environ. Eng.* 1998, 124 (6), 491–498.
- (14) Kim, H.; Rao P. S. C.; Annable, M. D. *Water Resour. Res.* 1997, 33 (12), 270–271.
- (15) Rao, P. S. C.; Annable, M. D.; Sillan, R. K.; Dai, D.; Hatfield, K.; Graham, W. D. *Water Resour. Res.* 1997, 33 (12), 2673–2686.
- (16) Jawitz, J. W.; Annable, M. D.; Rao, P. S. C.; Rhue, R. D. *Environ. Sci. Technol.* 1998, 32, 523–530.
- (17) McCray, J. E.; Brusseau, M. L. *Environ. Sci. Technol.* 1998, 32, 1285–1293.
- (18) Wilson, R. D.; Mackay, D. M. *Ground Water* 1993, 31 (5), 719–725.
- (19) Nelson, N. T.; Brusseau, M. L. *Environ. Sci. Technol.* 1996, 30 (9), 2589–2863.
- (20) Hunkeler, D.; Hoehn, E.; Hohener, P.; Zeyer, J. *Environ. Sci. Technol.* 1997, 31 (11), 3180–3187.
- (21) Tang, J. S.; Harker, B. *J. Can. Pet. Technol.* 1991, 30 (3), 76–85.
- (22) Tang, J. S.; Harker, B. *J. Can. Pet. Technol.* 1991, 30 (4), 34–42.
- (23) Studer, J. E. In *In Situ and On Site Bioremediation*; Alleman, B. C., Leeson, A., Eds.; Battelle Press: Columbus, OH, 1997; Vol. 4 (2), pp 345–351.
- (24) Deeds, N. E.; Pope, G. A.; McKinney, D. C. *Environ. Sci. Technol.* 1999, 33 (16), 2745–2751.
- (25) Kim, H.; Rao P. S. C.; Annable, M. D. *J. Contam. Hydrol.* 1999, 40 (1), 79–94.
- (26) Londergan, J. T.; Pope, G. A.; Brown, L. C.; Meinardus, H. W. *Proceedings, Petroleum Hydrocarbons and Organic Chemicals in Groundwater: Prevention, Detection, and Remediation Conference*, Houston, TX, 1997.
- (27) Young, C. M.; Jackson, R. E.; Jin, M.; Londergan, J. T.; Mariner, P. E.; Pope, G. A.; Anderson, F. J.; Houk, T. *Ground Water Monit. Rem.* 1999, 19 (1), 84–94.
- (28) James, A. I.; Graham, W. D.; Hatfield, K.; Rao, P. S. C.; Annable, M. D. *Water Resour. Res.* 1997, 33 (12), 2621–2636.
- (29) Barth, G. R.; Illangasekare, T. H.; Hill, M. C.; Rajaram, H. *Water Resour. Res.* 2001, 37, 21–31.
- (30) Chao, H.-C.; Rajaram, H.; Illangasekare, T. H. *Water Resour. Res.* 2000, 36, 2869–2878.
- (31) Ambwani, D. S.; Fort, T. In *Surface and Colloid Science*; Good R. J., Stromberg, R. R., Eds.; Plenum: New York, 1979; Vol. 11, Chapter 3.
- (32) Valocchi, A. J. *Water Resour. Res.* 1985, 21 (6), 808–820.

Received for review March 14, 2001. Revised manuscript received September 6, 2001. Accepted September 13, 2001.

ES010745K